# Theoretical interpretation of frequency sweeping observations in the Mega-Amp Spherical Tokamak

R. G. L. Vann
*Department of Physics, University of Warwick, Coventry CV4 7AL, United Kingdom*

R. O. Dendy
*Euratom/UKAEA Fusion Association, Culham Science Centre, Abingdon, Oxfordshire OX14 3DB, United Kingdom and Department of Physics, University of Warwick, Coventry CV4 7AL, United Kingdom*

M. P. Gryaznevich
*Euratom/UKAEA Fusion Association, Culham Science Centre, Abingdon, Oxfordshire OX14 3DB, United Kingdom*

(Received 5 October 2004; accepted 1 December 2004; published online 4 February 2005)

Frequency sweeping (chirping) of high frequency magnetohydrodynamic modes is widely observed in tokamak plasmas. In this paper observations of chirping in neutral-beam-heated plasmas in the Mega-Amp Spherical Tokamak (MAST) [A. Sykes, R. J. Akers, L. C. Appel *et al.*, Nucl. Fusion **41**, 1423 (2001)] are considered, and it is shown that these may be interpreted using the Berk–Breizman augmentation of the Vlasov–Maxwell equations. This model includes an energetic particle source: it leads not only to a single chirp but also to a series of bursting events. This repetitious behavior is characteristic of the chirping seen in experiments such as MAST. The similarity between features in velocity space and features in frequency space reinforces the theory that hole-clump pair formation is responsible for the observed frequency sweeping. © *2005 American Institute of Physics*. [DOI: 10.1063/1.1851991]

## I. INTRODUCTION

The coupling between energetic particle populations and high frequency magnetohydrodynamic (MHD) behavior is of considerable interest for tokamak plasmas. Spherical tokamaks, such as conventional aspect ratio tokamaks, display rich phenomenology in this area.[1–5] In this paper we focus on frequency sweeping (chirping) of high frequency MHD modes, which is widely observed in tokamak plasmas. Specifically, we consider observations (Fig. 1) of frequency chirping on the Mega-Amp Spherical Tokamak (MAST),[6] and show how these may be interpreted using the Berk–Breizman augmentation of the Vlasov–Maxwell equations [henceforth "the VM(BB) system"],[7] described below.

Figure 1 shows a plot of frequency (in the 100 kHz range) versus time (over an interval $\sim$10 ms) for MAST pulse 5568. This tokamak plasma was subjected to $P_{\mathrm{inj}}=950$ kW of D–D neutral beam heating at $\mathcal{E}_{\mathrm{inj}}=40$ keV beginning at time $t=0$, before the start ($t_0=62$ ms) of Fig. 1. Bulk plasma parameters for this discharge at time $t=50$ ms are central electron temperature $T_e=700$ eV, densities $n_i \approx n_e \approx 1.5\times10^{19}$ m$^{-3}$, toroidal magnetic field strength $B_\phi=0.46$ T, and plasma current $I=700$ kA. The Alfvén velocity in the core of the plasma is approximately $v_A=B_0/\sqrt{\mu_0\rho}=2.2\times10^6$ ms$^{-1}$. Energetic (40 keV) ion speed is $v_i=\sqrt{2\mathcal{E}_{\mathrm{inj}}/m_i}=2.2\times10^6$ ms$^{-1}$ at injection. It follows that a distinct, persistent, near-Alfvénic energetic ion population is created by neutral beam heating in this MAST plasma. This motivates the interpretation of the observed high frequency MHD behavior (Fig. 1) in terms of the VM(BB) model.

Let us briefly estimate the energy and number density of the injected ion population. The energy density $W_{\mathrm{inj}}$ of injected particles can be approximated by

$$W_{\mathrm{inj}} \sim \frac{P_{\mathrm{inj}}\tau_{\mathrm{inj}}}{V_{\mathrm{MAST}}} \sim 1.3\left(\frac{\tau_{\mathrm{inj}}}{\tau_{\mathrm{MAST}}}\right)\ \mathrm{kJ\ m^{-3}}; \tag{1}$$

here $\tau_{\mathrm{inj}}$ denotes the mean confinement time of injected ions, and we use values of the plasma volume $V_{\mathrm{MAST}}=10$ m$^3$ and energy confinement time $\tau_{\mathrm{MAST}}=14$ ms$\pm2$ ms for MAST from Ref. 6, with $P_{\mathrm{inj}}=950$ kW as above.

The energy density of the background thermal deuteron population

$$W_{\mathrm{th}} \sim n_{\mathrm{th}}T_{\mathrm{th}} \sim 1.7\left(\frac{T_{\mathrm{th}}}{T_{\mathrm{e}}}\right)\ \mathrm{kJ\ m^{-3}} \tag{2}$$

making the approximation $n_{\mathrm{th}}\approx n_{\mathrm{i}}\approx n_{\mathrm{e}}$ and inserting the measured values given above for the electron temperature $T_{\mathrm{e}}$ and electron density $n_{\mathrm{e}}$. This implies that the ratio of energy densities in the bulk and injected ion populations is given by

$$\frac{W_{\mathrm{inj}}}{W_{\mathrm{th}}} \sim 0.8\left(\frac{T_{\mathrm{e}}}{T_{\mathrm{th}}}\right)\left(\frac{\tau_{\mathrm{inj}}}{\tau_{\mathrm{MAST}}}\right). \tag{3}$$

Similarly, applying $W_{\mathrm{inj}}\sim n_{\mathrm{inj}}\mathcal{E}_{\mathrm{inj}}$, we obtain the ratio

$$\frac{n_{\mathrm{inj}}}{n_{\mathrm{th}}} \sim \frac{W_{\mathrm{inj}}}{n_{\mathrm{th}}\mathcal{E}_{\mathrm{inj}}} \sim 0.014\left(\frac{\tau_{\mathrm{inj}}}{\tau_{\mathrm{MAST}}}\right) \tag{4}$$

by again approximating $n_{\mathrm{th}}\sim n_{\mathrm{i}}\sim n_{\mathrm{e}}$, substituting for $W_{\mathrm{inj}}$ from Eq. (1), and taking the given value for $\mathcal{E}_{\mathrm{inj}}$. The dimensionless parameters $T_{\mathrm{e}}/T_{\mathrm{th}}$ and $\tau_{\mathrm{inj}}/\tau_{\mathrm{MAST}}$ are of order unity. We may conclude that in a MAST plasma of the kind considered, $W_{\mathrm{inj}}\sim W_{\mathrm{th}}$ and $n_{\mathrm{inj}}\sim 0.01 n_{\mathrm{th}}$.

 

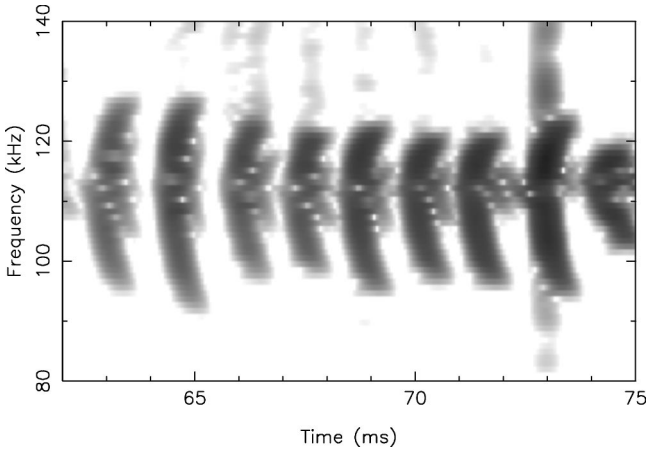


FIG. 1. Experimental observation of frequency chirping in nine successive bursts of high frequency MHD activity. Magnitude of MHD activity measured in a neutral beam-heated MAST pulse 5568 during a 13 ms interval, showing frequency in the range 80 kHz–140 kHz. Logarithmic gray scale plot spanning two orders of magnitude.

The data shown in Fig. 1 are obtained from three Mirnov coils in the midplane of MAST with a sampling rate of 1 MHz. Comparison of the phase of the data between the coils implies that the dominant mode has toroidal mode number $n=1$. Having deduced the toroidal wave number, and already knowing the toroidal angular separation of the coils, we can decompose the data observed at any one coil into components moving clockwise and anticlockwise, as described in Appendix A.

The primary observational features of Fig. 1, whose modeling we address in this paper, include the following.

(1) There are nine repeated bursts of MHD activity, each lasting $\approx 0.8$ ms. Each burst is separated from its predecessor by a brief quiescent period. The time interval between onset of successive bursts is 1.2 ms. The initial frequencies of all the bursts are closely similar: there is a characteristic frequency $\sim 110$ kHz.

(2) During a single burst, the characteristic frequency evolves with time, "chirping." In Fig. 1, the bursts exhibit approximately symmetric up-down chirping. Over the lifetime of the burst (0.8 ms), the frequency changes by $\approx \pm 15$ kHz, which corresponds to a proportional change of $\pm 14\%$. This frequency change takes place in a plasma whose bulk properties are quasistationary at this time. For this reason, a mechanism for chirping is sought in terms of the self-consistent time evolution of the energetic ion population and its associated MHD modes.

The dominant high frequency MHD mode shown in Fig. 1 is identified as a toroidal Alfvén eigenmode excited by the energetic ion population and reacting back upon it. The self-consistent evolution of such a system can be modeled by the VM(BB) system,[8] which we now briefly outline. The VM(BB) system models the coupling between energetic particles and the wave modes they excite, based on the one-dimensional electrostatic bump-on-tail model with particle distribution relaxation and background electric field damping. We cast the model as follows,[9] in terms of the particle distribution $f(x,v,t)$ and the electric field $E(x,t)$:

$$\frac{\partial f}{\partial t} + v\frac{\partial f}{\partial x} + E\frac{\partial f}{\partial v} = -\nu_a(f - F_0), \tag{5}$$

$$\frac{\partial E}{\partial t} + \int v(f - f_0)dv = -\gamma_d E. \tag{6}$$

Here $F_0$ denotes the combined particle source and loss function, $\nu_a$ the particle relaxation rate, $\gamma_d$ the combined effect of all background damping mechanisms that act on the electric field, and $f_0$ the spatial mean of $f$. Spatial lengths are normalized to the debye length $\lambda_D$, velocities to the thermal speed $v_{\text{the}}$, time to the inverse plasma frequency $\omega_p^{-1} \equiv \lambda_D / v_{\text{the}}$, and $E$ to $m_e v_{\text{the}}^2 / e\lambda_D$. Central to the present paper is an interpretive code[9,10] which uniquely solves the fully nonlinear VM(BB) system without employing analytical approximations. It allows direct numerical solutions of the fully nonlinear VM(BB) system across the entirety of $(\gamma_d, \nu_a)$ parameter space for any $F_0(v)$. Application of this code[9] for a particular $F_0(v)$ shows how the behavior of the VM(BB) system depends on its parameters. Conversely it enables one to map time-dependent wave phenomenology to evolving structures in velocity space. Our objective is to investigate how far the conceptually simple physics basis of the VM(BB) model captures the observed phenomenology of MAST MHD bursts. As we shall see, the model appears remarkably successful, and the role of hole-clump pairs becomes particularly apparent.

## II. DISCUSSION AND IMPLEMENTATION OF THE VM(BB) MODEL

It is helpful to review the structure of the VM(BB) system of equations, Eqs. (5) and (6), from a fully nonlinear and computational perspective, noting that previous work[7,11] typically applies to limiting regimes where analytically tractable ordering schemes can be deployed. Let us consider first the distribution $F_0(v)$, to which $f(x,v,t)$ seeks to relax at all positions $x$. Physically, as BB have described, $F_0(v)$ is determined by the balance of the energetic particle source rate $Q(v)$ with the loss rate $\nu_a$. Specifically the right-hand side of Eq. (5) may be written

$$-\nu_a(f - F_0) = Q(v) - \nu_a f \tag{7}$$

such that $F_0 = Q/\nu_a$. In the present study, we choose a third way of expressing this physics, such that Eq. (5) becomes

$$\mathcal{D}_t f = Q_{\text{energetic}}(v) - \nu_a[f(x,v,t) - f_{\text{Maxwellian}}(v)], \tag{8}$$

where the Lagrangian phase-space derivative $\mathcal{D}_t = \partial_t + v\partial_x + E\partial_v$. In Eq. (8), the velocity distribution relaxes explicitly towards a Maxwellian at a rate $\nu_a$, and is driven by the spatially uniform particle source term $Q_{\text{energetic}}(v)$. The function $Q_{\text{energetic}}(v)$ in Eq. (8) differs from its counterpart $Q(v)$ in Eq. (7) because of the way in which we have formulated the relaxation process. Specifically, $Q_{\text{energetic}}(v) = Q(v) - \nu_a f_{\text{Maxwellian}}(v)$. We note that all of the formulations that we have discussed are mathematically and physically equivalent, and are fully nonlinear.

When implementing the VM(BB) system numerically, one must therefore choose a form for $F_0(v)$, or equivalently

for $Q_{\text{energetic}}(v)$ and $f_{\text{Maxwellian}}(v)$, in addition to values for the model parameters $\nu_a$ and $\gamma_d$. There remains a further choice: the initial shape of the distribution $f(x,v,t=0)$ and the electric field $E(x,t=0)$. In the present fully nonlinear implementation, $f(x,v,t)$ can deviate arbitrarily from $F_0(v)$, whereas most analytical developments of the VM(BB) system treat $f-F_0$ as a small parameter. The value chosen for $f(x,v,t=0)$ does not, in principle, affect the long-term evolution of the system, which is governed by the three degrees of freedom $\nu_a$, $\gamma_d$, and $F_0(v)$. For the present application, we initialize such that the basic structure of the beam population is preserved throughout the simulation. Specifically we choose $F_0$ to be the sum of two Gaussian distributions,

$$F_0(v) = F_{\text{bulk}} + F_{\text{beam}}, \tag{9}$$

where

$$(2\pi)^{1/2} F_{\text{bulk}} = (\eta/v_c)\exp(-v^2/2v_c^2), \tag{10}$$

$$(2\pi)^{1/2} F_{\text{beam}} = [(1-\eta)/v_t]\exp[-(v-v_b)^2/2v_t^2], \tag{11}$$

and we choose $\eta=0.96$, $v_c=0.1$, $v_b=6.0$, and $v_t=2.0$. In the case $\gamma_d=\nu_a=0$, direct numerical solution of the Landau dispersion relation gives us the initial linear instability growth rate $\gamma_L=0.0494$ and frequency $\omega_L=0.961$. The subscript "bulk" in Eqs. (9) and (10) refers to injected ions that have become quasithermalized, which do not necessarily account for all of the thermal ions in the plasma.

The way in which the behavior of the VM(BB) system depends on the fundamental model parameters $(\gamma_d,\nu_a)$ has recently been analyzed systematically in the fully nonlinear regime.[9,10] In particular, it has been shown that the system exhibits four distinct types of behavior (damped, steady state, periodic, and chaotic), which each occur in well defined regions of parameter space. The frequency sweeping behavior described in this paper is found to occur within the chaotic regime. For this empirical reason, the fundamental model parameters are fixed throughout the simulation (corresponding to a steady source and damping) at $(\gamma_d,\nu_a)=(0.1,0.0001)$. These parameters result in a decreased initial linear instability drive $\gamma=0.007\,06$. The real frequency is modified slightly, to $\omega=0.965$, so that the resonant phase velocity $v_\phi=\omega/k=3.86$.

The version of the code used to generate the simulation results in this paper has been parallelized using the Message Passing Interface.[12] It divides velocity space into a number of equally sized regions, each of which is dealt with by a separate processor. The velocity advection requires the transmission of "ghost cells" between adjacent regions. The simulations are performed on a cluster of 1.4 GHz nodes at the Centre for Scientific Computing at the University of Warwick. The computational time-stepping rate achieved is $\approx 10^6$ points per processor per second, so that a simulation of duration $10^6\omega_p^{-1}$ running on 32 processors takes approximately one week of machine time.

The simulations in this paper are performed on a spatially periodic grid with $N_x=256$, $L=8\pi$, $N_v=2048$, $v_{\min}=-10$, and $v_{\max}=22$. The initial distribution $f(x,v,t=0)=F_0(v)[1+\alpha\cos(x/4)]$. The initial electric field is then provided by Poisson's equation $E(x,t=0)=4\alpha\sin(x/4)$. The initial spatial perturbation amplitude $\alpha$ is chosen to be $10^{-6}$.

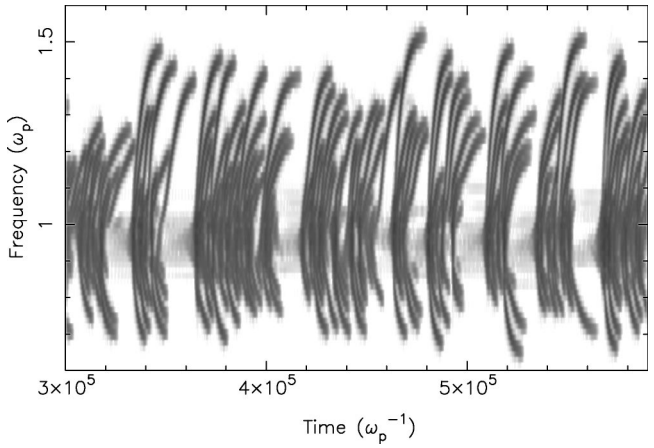


FIG. 2. Frequency chirping in successive bursts of activity from the fully nonlinear VM(BB) model. Dimensionless time and frequency are normalized by $\omega_p$. Logarithmic gray scale plot of amplitude of Hanning-windowed fast Fourier transform across three orders of magnitude.

## III. RESULTS AND DISCUSSION

Figure 2 shows the time evolution of the frequency of the first spatial mode for the fully nonlinear VM(BB) system during an interval lasting $\approx 3\times 10^5\omega_p^{-1}$. Figure 3 focuses on a specific episode within Fig. 2, lasting $\approx 2.5\times 10^4\omega_p^{-1}$. Recall that the two control parameters $\nu_a$ and $\gamma_d$ are fixed throughout the simulation, corresponding to a quasistationary background plasma and energetic particle drive. Time evolution of the system thus arises solely from the self-consistent interaction of the energetic particle population and its associated field.

Like Fig. 1, Fig. 2 exhibits repeated bursts whose frequency undergoes almost-symmetric up-down chirping. Plots of the spatially averaged distribution function $f_0(v)$, linked to corresponding instants during the evolution of the single

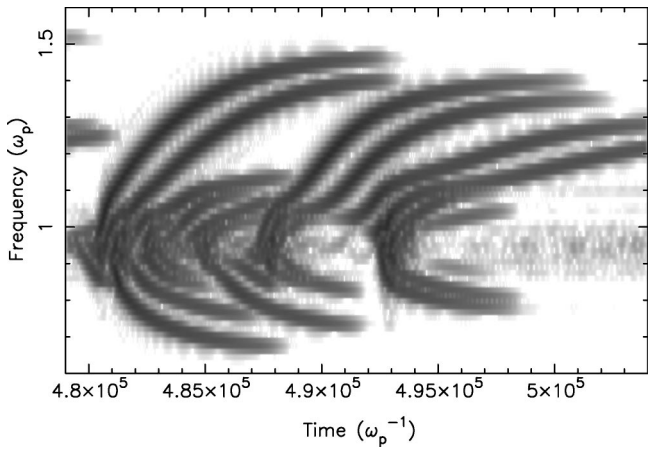


FIG. 3. Time evolution of frequency during the second burst of activity that occurs in the VM(BB) model from Fig. 2, time interval $4.79\times 10^5 < t < 5.04\times 10^5$. Dimensionless time and frequency are normalized by $\omega_p$. Logarithmic gray scale plot. Key episodes in the associated hole-clump pair evolution of $f_0(v)$ are plotted in Fig. 4.

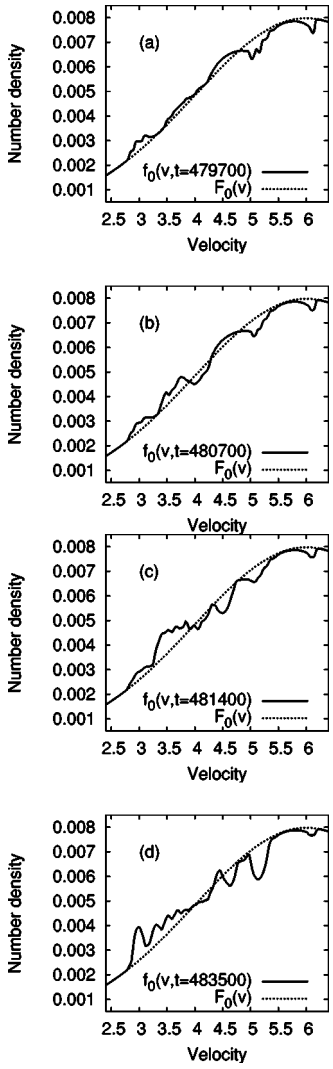


FIG. 4. Hole-clump pair formation and evolution, shown at four times during the single burst of chirping activity shown in Fig. 3. Horizontal axis plots velocity in the range $2.4<v<6.4$, which corresponds to the $\partial f/\partial v>0$ beam region of the initial spatially averaged distribution $f_0(v,t=0)$; the resonant velocity is at $v=3.86$. Vertical axis plots spatially averaged $f(v)$. Panel (a) is from a period of quiescence; note that $f_0 \approx F_0$. The first stage of hole-clump formation is the gradient inversion at the resonant velocity as seen in panel (b). This corresponds to the first phase-space half rotation of trapped particles in the resonant region. The phase-space mixing becomes increasingly complex in panel (c). Panel (d) shows well-developed holes (above the resonant velocity) and clumps (below the resonant velocity).

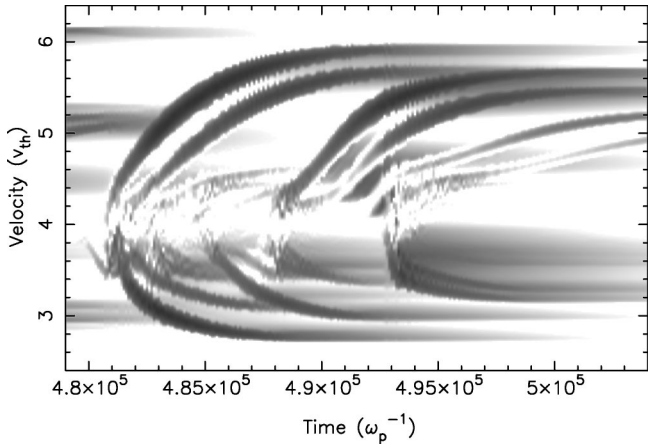


FIG. 5. Hole-clump evolution shown for the same time range as Fig. 3. The plot shows $\ln|f_0(v,t)-F_0(v)|$ as a function of velocity on the vertical axis and time on the horizontal axis.

burst shown also in Fig. 3, are displayed in Fig. 4. This demonstrates the central role of hole-clump pair formation and evolution as we now describe.

Panel (a) of Fig. 4 corresponds to a period of inactivity. We note that the spatially averaged distribution $f_0(v)$ differs only slightly from the equilibrium bump-on-tail distribution $F_0(v)$. In particular, the gradients of the two distributions at the resonant velocity $v=3.86$ are approximately equal, so this configuration is linearly unstable.

Panel (b) shows the first stage of hole-clump formation: velocity gradient inversion of $f_0(v)$ at the resonant velocity $v=3.86$. This gradient inversion is due to the first nearly synchronized half rotation in phase space of particles in the potential well formed by the linear instability. More complete phase-space mixing in the region $3.5 \leqslant v \leqslant 4$ is shown in panel (c). It appears as a flattening of the distribution function in this interval. The wave mode's potential well is not parabolic, so that particles of different energies with respect to the rest frame of the wave will oscillate in the wave's potential well at slightly different frequencies, which after several rotations leads to phase-mixed particle trajectories.

Panel (d) shows hole-clump pair formation. Two hole-clump pairs are particulary well defined at $(v_{\text{clump}}, v_{\text{hole}}) = (3.0, 5.2)$ and $(v_{\text{clump}}, v_{\text{hole}}) = (3.3, 4.6)$. Each clump, i.e., surplus of particles relative to the equilibrium solution $F_0(v)$ is situated below the resonant velocity. Each hole, i.e., deficit of particles in $f_0(v)$ relative to $F_0(v)$ is situated above the resonant velocity. The holes and clumps each move in velocity space quasisymmetrically away from the resonant velocity as time proceeds.

The snapshots shown in Fig. 4 are complemented by the continuous time evolution plot of the distribution function shown in Fig. 5. This is plotted in terms of $\ln|f_0(v,t) - F_0(v)|$, so as to provide visual emphasis for hole-clump pairs. The close correlation between evolving structures in frequency (Fig. 3) and velocity (Fig. 5) is noteworthy. Since the activity occurs at fixed $k=0.25$, there is a direct map from phase-velocity to frequency via the relation $\omega = k v_\phi$. Hence there is a one-to-one correspondence between the features in the frequency plot Fig. 3 and the plot of distribution function perturbation Fig. 5. This leads us to conclude that hole-clump formation is entirely responsible for the features seen in frequency space. We therefore suggest that the hole-clump formation observed directly in our simulation also occurs in MAST, and that this evolution of the distribution function is responsible for the frequency chirping seen in Fig. 1.

Deeper theoretical understanding of hole-clump formation and evolution can be obtained by measuring how the amplitude and frequency of the chirping features vary in time for data such as that in Fig. 3. The first stage is to isolate each of the "fronds." This is done by identifying maxima with respect to frequency at each time. The amplitude associated with each frequency maximum is then calculated as

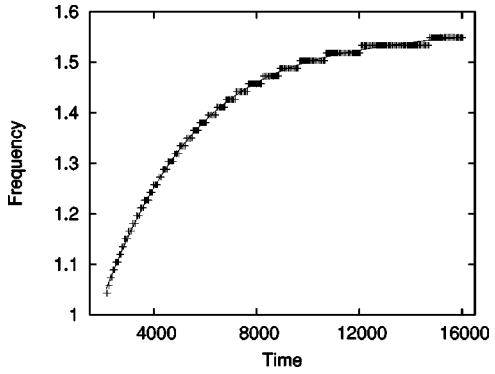


FIG. 6. A single frequency-sweeping frond isolated for analysis. The crosses show the points of maximum amplitude as a function of time. The solid line is the best-fit quartic to the data points.

the integral of the signal between the two adjacent minima. Fronds are isolated by testing for connectedness between adjacent points in time; an example from simulation is shown in Fig. 6. The curve-fitting algorithm described in Appendix B is then applied. While earlier analytically based hole-clump work[11] yields $\delta\omega \propto t^{1/2}$, we find that the frequency-time relationship is better described by an exponential model in this fully nonlinear regime, well separated from the linear instability threshold. However, these curve fittings, despite being useful at relatively large times (distant from hole-clump birth), do not necessarily yield information on initial behavior or creation. For a discussion of frequency-time evolution of Alfvén eigenmodes modeled by the HAGIS code, we refer to Ref. 13.

## IV. CONCLUSION

In this paper we show that the fully nonlinear self-consistent VM(BB) system, Eqs. (5) and (6), exhibits frequency sweeping. This frequency sweeping (chirping) occurs for model parameters corresponding to the chaotic regime identified in Ref. 9. This model, in contrast to previous work,[11] includes an energetic particle source: it leads not only to a single chirp, but to a series of bursting events. This repetitious behavior is characteristic of the chirping seen in experiments such as MAST (Fig. 1). The striking similarity between features in velocity space [specifically in the distribution perturbation $f_0(v)-F_0(v)$] and features in frequency space reinforces the theory that hole-clump pair formation is responsible for the observed frequency sweeping.

We have developed a technique for isolating frequency-sweeping fronds, and fitting the resulting frequency-time or amplitude-time data to simple model relationships (see Appendix B). Preliminary analysis suggests that our simulation results may not fit the $\delta\omega \propto t^{1/2}$ relationship proposed by near-threshold models.[7] This prompts discussion of what regime is being exhibited by the experiment, however the currently available MAST data, sampled at 1 MHz, does not reveal the fine structure of the chirping modes at sufficient resolution to give a definitive answer. For the future, we note that the relevant diagnostics on MAST are capable of acquiring data at 10 MHz. Such experiments could reveal which model parameter regime is most relevant. Further development of numerical techniques (e.g., Ref. 14) is also necessary to maximise the information that can be gathered from noisy experimental and simulation data. There is also scope for further theoretical work. Simulation measurements of $f_0(v)$ will help to build upon existing theories of hole-clump formation.[15] It would be useful to investigate why two hole-clump pairs are often created together, see, for example, the pairs of holes and pairs of clumps that move nearly parallel to each other in Fig. 3.

## ACKNOWLEDGMENTS

The authors would like to thank Professor Boris Breizman and Professor Herb Berk for helpful discussions. This work was supported in part by Euratom and the UK Engineering and Physical Sciences Research Council. Computing facilities were provided by the Centre for Scientific Computing of the University of Warwick with support from Joint Research Equipment Initiative Grant No. JR00WASTEQ.

## APPENDIX A: LEFT-RIGHT WAVE DECOMPOSITION

Let $X_+$ and $X_-$ denote the components of a wave moving forwards and backwards with respect to increasing phase $\phi$. The data observed at two coils with a known phase difference of $\Delta\phi > 0$ can then be written

$$A_0(t) = X_+(t) + X_-(t), \tag{A1}$$

$$A_1(t) = X_+(t - \Delta\phi/\omega) + X_-(t + \Delta\phi/\omega). \tag{A2}$$

This implies the relationship

$$\frac{\tilde{A}_0(\omega) - \tilde{A}_1(\omega)e^{i\Delta\phi}}{1 - e^{2i\Delta\phi}} = \begin{cases} \tilde{X}_+(\omega) & \text{if } \omega < 0, \\ \tilde{X}_-(\omega) & \text{if } \omega > 0, \end{cases} \tag{A3}$$

where the tilde represents the Fourier transform with respect to time. We seek the signal's frequency spectrum as a function of time. This can be done either using wavelet analysis or by using a windowed Fourier transform. Here we apply the second approach, convolving the measured signal with the Hanning function $H(t;T) = \sin^2(\pi t/T)$ in the Fourier transform (the shaped window eliminates spurious boundary effects),

$$\tilde{A}(\omega;t) = \int_t^{t+T} H(\tau;T)A(\tau)\exp(-i\omega\tau)d\tau. \tag{A4}$$

The window length $T$ has to be chosen carefully in order to obtain a useful spectrogram. For the MAST data in question we choose $T = 1024$ sampling periods.

## APPENDIX B: PRINCIPLES OF SPECIALIZED CURVE FITTING

Fitting a simple curve, such as a power law or exponential, to data from an experiment or simulation typically involves three or four free parameters. These determine an origin shift, stretch of axes, and an exponent or power. Let us

write the fitting function as $f(x;\lambda_i)$ and the data as the set of $N$ points $(x_j,y_j):1\leqslant j\leqslant N$, where the second coordinate is assumed to depend on the perfectly known first coordinate. The problem is then to solve for the $\lambda_i$ so as to minimize the distance

$$d(\lambda_i)=\sum_{j=1}^{N}[f(x_j;\lambda_i)-y_j]^2. \tag{B1}$$

This is an optimization problem in three or four dimensions with a cost function of $N$ terms. For realistic $N\sim 100$, $d(\lambda_i)$ usually has many local minima and so the problem is computationally expensive to solve.

A more efficient algorithm is as follows. Let us assume that the data $(x_j,y_j)$ have only one or two extrema and that $N\gg 10$. Then it is possible (and cheap) to fit a mid-order (e.g., fourth order) polynomial $p(x)$ to the data. We then redefine the distance to be

$$d(\lambda_i)=\int_a^b[f(x;\lambda_i)-p(x)]^2, \tag{B2}$$

where $a$ and $b$ are the minimum and maximum values, respectively, of $x_j$ over $1\leqslant j\leqslant N$. The function $d(\lambda_i)$ can then be differentiated with respect to each of the $\lambda_i$, thus reducing the optimization problem to the solution of three or four simultaneous equations.

[1] K. G. McClements, M. P. Gryaznevich, S. E. Sharapov, R. J. Akers, L. C. Appel, G. F. Counsell, C. M. Roach, and R. Majeski, Plasma Phys. Controlled Fusion **41**, 661 (1999).
[2] M. P. Gryaznevich and S. E. Sharapov, Nucl. Fusion **40**, 907 (2000).
[3] E. D. Fredrickson, N. Gorelenkov, C. Z. Cheng, R. Bell, D. Darrow, D. Johnson, S. Kaye, B. LeBlanc, J. Menard, S. Kubota, and W. Peebles, Phys. Rev. Lett. **87**, 145001 (2001).
[4] M. P. Gryaznevich and S. E. Sharapov, Plasma Phys. Controlled Fusion **46**, S15 (2004).
[5] JET-EFDA Contributors, S. D. Pinches, H. L. Berk, D. N. Borba, B. N. Breizman, S. Briguglio, A. Fasoli, G. Fogaccia, M. Gryaznevich, V. Kiptily, M. Mantsinen, S. E. Sharapov, D. Testa, R. G. L. Vann, G. Vlad, and F. Zonca, Plasma Phys. Controlled Fusion **46**, B187 (2004).
[6] A. Sykes, R. J. Akers, L. C. Appel *et al.*, Nucl. Fusion **41**, 1423 (2001).
[7] H. L. Berk, B. N. Breizman, J. Candy, M. Pekker, and N. V. Petviashvili, Phys. Plasmas **6**, 3102 (1999).
[8] H. L. Berk and B. N. Breizman, Phys. Fluids B **2**, 2226 (1990); **2**, 2235 (1990); **2**, 2246 (1990).
[9] R. G. L. Vann, R. O. Dendy, G. Rowlands, T. D. Arber and N. d'Ambrumenil, Phys. Plasmas **10**, 623 (2003).
[10] T. D. Arber and R. G. L. Vann, J. Comput. Phys. **180**, 339 (2002).
[11] H. L. Berk, B. N. Breizman, and N. V. Petviashvili, Phys. Lett. A **234**, 213 (1997); **238**, 408 (1998).
[12] W. Gropp, E. Lusk, N. Doss, and A. Skjellum, Parallel Comput. **22**, 789 (1996).
[13] JET-EFDA Contributors, S. D. Pinches, H. L. Berk, M. P. Gryaznevich, and S. E. Sharapov, Plasma Phys. Controlled Fusion **46**, S47 (2004).
[14] EFDA-JET Contributors, A. C. A. Figueiredo, and M. F. F. Nave, "Improved time-frequency visualization of chirping mode signals in tokamak plasmas using the Choi-Williams distribution," IEEE Trans. Plasma Sci. (submitted).
[15] D. Yu. Eremin and H. L. Berk, Phys. Plasmas **9**, 772 (2002).